

Large fluctuations in NSPT computations: a lesson from $O(N)$ non-linear sigma models

Paolo Baglioni^{a,b} and Francesco Di Renzo^{a,b}

^aDipartimento di Scienze Matematiche, Fisiche e Informatiche, Università di Parma

^bINFN, Gruppo Collegato di Parma

Abstract

In the last three decades, Numerical Stochastic Perturbation Theory (NSPT) has proven to be an excellent tool for calculating perturbative expansions in theories such as Lattice QCD, for which standard, diagrammatic perturbation theory is known to be cumbersome. Despite the significant success of this stochastic method and the improvements made in recent years, NSPT apparently cannot be successfully implemented in low-dimensional models due to the emergence of huge statistical fluctuations: as the perturbative order gets higher, the signal to noise ratio is simply not good enough. This does not come as a surprise, but on very general grounds, one would expect that the larger the number of degrees of freedom, the less severe the fluctuations will be. By simulating $2D$ $O(N)$ non-linear sigma models for different values of N , we show that indeed the fluctuations are tamed in the large N limit, meeting our expectations. Having established this, we conclude discussing interesting applications of NSPT in the context of these theories.

1 Introduction

Lattice regularization of a field theory represents today one of the primary methods for investigating non-perturbative phenomena in theories that are too complex to study with analytical methods, such as QCD. The constant development of new MonteCarlo algorithms, combined with the improvements of hardware resources, has made non-perturbative numerical calculations accessible, which were previously beyond reach using non-numerical strategies. Quite interestingly, it is also possible to numerically implement stochastic algorithms for perturbation theory that are *in practice* quite close to the machinery of non-perturbative simulations. The most well-known and fruitful tool is Numerical Stochastic Perturbation Theory (NSPT). Initially introduced in the '90s [1] as a numerical implementation of Parisi and Wu's Stochastic Quantization [2], today it is available in various (more or less) equivalent formulations [3, 4]. In particular, NSPT provides a direct pathway to the numerical computation of very general observables in Lattice QCD at perturbative orders that have never been explored analytically [5, 6, 7]. NSPT's success can (also) be attributed to its systematic and efficient numerical automation of order-by-order operations [8], exactly in the same way as in what has become in recent times quite popular under the name of Automatic Differentiation (see *e.g.* [9]).

Since the initial introduction of NSPT, considerable expertise has been gathered, aiming in particular at a deeper comprehension of the underlying stochastic process. This interest was significantly triggered by the observation that, when applied to *small systems* (in a sense that will be clear in the following), NSPT produced huge fluctuations (not normally distributed) at orders that the method could successfully manage to compute for *larger ones* [10].

In this work we investigate how to make more quantitative the observation that the presence of large deviations at high perturbative orders can be related to the density of degrees of freedom of the system at hand. This conjecture finds an ideal testing ground in the study of $O(N)$ non-linear sigma models (NLSM). A tendency of distributions of NSPT computed coefficients to Gaussian in a large N limit has already been reported (at low orders) in [11]. Our strategy will enable us to identify regimes (*i.e.* values of N) in which the model can be safely simulated and reliable predictions can be made. All in all, the scenario is that depicted in Fig. 1: NSPT computations are safe in the large N limit (while at each value of N we can afford reliable computations up to a maximum loop order n).

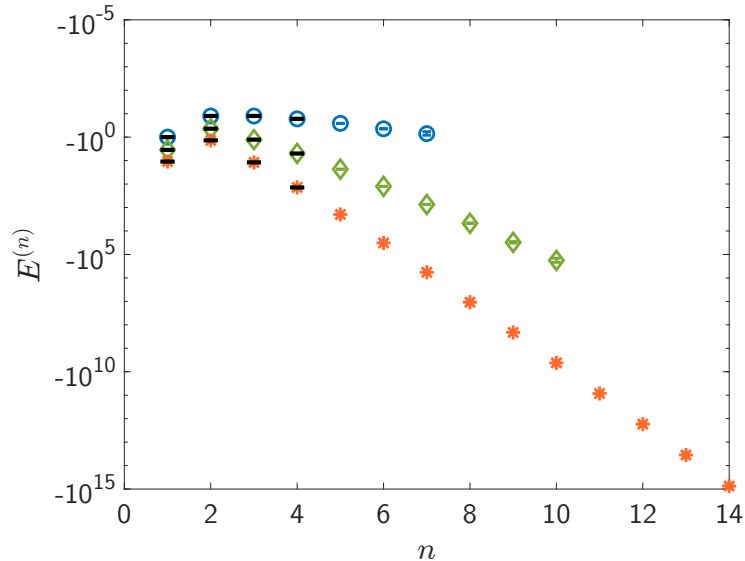


Figure 1: The main message of this work as seen in NSPT perturbative computations in $O(N)$ non-linear sigma models: the energy of the model is computed at increasing perturbative order n ; blue symbols refer to $O(5)$, green ones to $O(15)$, orange ones to $O(45)$ (known analytic results are in black). While increasing fluctuations prevent us from safely computing high orders at *small* N , the larger is N , the higher loop we can safely compute.

This work is structured as follows: in Section 1 we provide a brief description of NSPT and the motivations behind this study; the large deviations issue will be introduced and a simple, natural conjecture will be presented. In Section 2 we introduce two-dimensional $O(N)$ non-linear sigma models, revisiting in particular the setup for perturbation theory. In Section 3 we present the onset of fluctuations at not-so-large N and how this effect is substantially tamed in the large N limit. Section 4 provides a more quantitative description based on the study of relative errors for different values of N ; by looking at the results of our study *a posteriori*, we will recognise criteria for assessing which N is large enough for successful NSPT computations at a given loop order. In Section 5 we conclude with some remarks and future prospects, in particular outlining potential opportunities for the study of asymptotic effects (*e.g.* renormalons, expansions around non-trivial vacua, resurgence).

1.1 Numerical Stochastic Perturbation Theory

NSPT was initially inspired by the famous work of Parisi and Wu [2] on Stochastic Quantization (SQ). With this respect, NSPT is basically a numerical implementation of stochastic perturbation theory (which was originally approached in a diagrammatic form; for a review see [12]). In short, NSPT is nothing more than the numerical integration of a tower of Langevin equations rewritten order-by-order, *i.e.* in perturbation theory. The mechanism underlying NSPT is actually more general and can be implemented starting from many stochastic differential equations [3, 4]. In the following, we will

adhere to the original formulation.

To be more precise, we can sketch the path from SQ to NSPT as follows. We are interested in calculating expectation values of a Euclidean field theory, namely

$$\langle O[\phi] \rangle = \frac{\int \mathcal{D}\phi \ O(\phi) \ e^{-\mathcal{S}_E[\phi]}}{\int \mathcal{D}\phi \ e^{-\mathcal{S}_E[\phi]}} \quad (1)$$

The basic idea is to promote the fields to functions of a new extra variable (known in the literature as stochastic time)

$$\phi(\mathbf{x}) \rightarrow \phi_\eta(\mathbf{x}, \tau) \quad (2)$$

and evolve the system in this fictitious time according to the Langevin stochastic equation

$$\frac{d\phi_\eta(\mathbf{x}, \tau)}{d\tau} = -\frac{\partial \mathcal{S}_E[\phi]}{\partial \phi_\eta(\mathbf{x}, \tau)} + \eta(\mathbf{x}, \tau) \quad (3)$$

where $\eta(\mathbf{x}, \tau)$ is a normalized Gaussian noise satisfying

$$\langle \eta(\mathbf{x}, \tau) \rangle_\eta = 0 \quad \langle \eta(\mathbf{x}, \tau) \eta(\mathbf{x}', \tau') \rangle_\eta = 2\delta(\mathbf{x} - \mathbf{x}')\delta(\tau - \tau') \quad (4)$$

In the previous equations, the symbol $\langle \dots \rangle_\eta$ means

$$\langle \dots \rangle_\eta = \frac{\int \mathcal{D}\eta \ \dots \ e^{-\frac{1}{4} \int d\mathbf{x} d\tau \eta^2(\mathbf{x}, \tau)}}{\int \mathcal{D}\eta \ e^{-\frac{1}{4} \int d\mathbf{x} d\tau \eta^2(\mathbf{x}, \tau)}} \quad (5)$$

while the subscript in $\phi_\eta(\mathbf{x}, \tau)$ denotes the dependence on the realization of the noise. The fundamental assertion of SQ is that the expectation value of an observable with respect to the noise in Eq. (5) reproduces, in the limit of infinite stochastic time, the expectation values of the Euclidean field theory we are interested in Eq. (1), that is

$$\lim_{\tau \rightarrow \infty} \langle O[\phi_\eta(\mathbf{x}_1, \tau), \phi_\eta(\mathbf{x}_2, \tau), \dots, \phi_\eta(\mathbf{x}_n, \tau)] \rangle_\eta = \langle O[\phi(\mathbf{x}_1), \phi(\mathbf{x}_2), \dots, \phi(\mathbf{x}_n)] \rangle \quad (6)$$

Because of Eq. (6), the numerical integration of Eq. (3) provides one of the algorithmic options for non-perturbative Monte Carlo simulations [13, 14]. In this context, the systematic error arising from the introduction of a finite time step can be eliminated by an additional *à la* Metropolis acceptance step [15]. On the other hand, NSPT takes the solution of Eq. (3) and expand it in a (formal) power series in the coupling constant (from now on, we will omit the subscript η for convenience):

$$\phi(\mathbf{x}, \tau) = \phi^{(0)}(\mathbf{x}, \tau) + \sum_{n=1}^{\infty} g^n \phi^{(n)}(\mathbf{x}, \tau) \quad (7)$$

It is easy to see that, by substituting the previous expression into Eq. (3) and recollecting the various orders in the coupling constant g , we obtain a tower of partial differential equations

$$\begin{aligned} \frac{d\phi^{(0)}(\mathbf{x}, \tau)}{d\tau} &= -G_0^{-1}\phi^{(0)}(\mathbf{x}, \tau) + \eta(\mathbf{x}, \tau) \\ \frac{d\phi^{(1)}(\mathbf{x}, \tau)}{d\tau} &= -G_0^{-1}\phi^{(1)}(\mathbf{x}, \tau) + D_1(\phi^{(0)}) \\ &\dots \\ \frac{d\phi^{(n)}(\mathbf{x}, \tau)}{d\tau} &= -G_0^{-1}\phi^{(n)}(\mathbf{x}, \tau) + D_n(\phi^{(0)}, \phi^{(1)}, \dots, \phi^{(n-1)}) \end{aligned} \quad (8)$$

where G_0^{-1} is the free propagator (*i.e.*, $\frac{\partial S_0[\phi]}{\partial \phi^{(0)}(\mathbf{x}, \tau)} = G_0^{-1} \phi^{(0)}(\mathbf{x}, \tau)$, where S_0 is the free Euclidean action) and D_n the interaction terms that mix different perturbative orders of the fields. It is worth noting that the truncation is exact at any order: the equation at a given perturbative order n only depends on the fields at order $n' \leq n$. Of course, the tower of equations must be integrated numerically with a given integrator and a given value of a time step. With this respect it is important to point out a practical difference between the non-perturbative solution of the Langevin equation and NSPT: in the latter case, we cannot introduce an acceptance step to eliminate systematic errors in the time step size. Instead, we will extrapolate results in the $\Delta\tau \rightarrow 0$ limit, the appropriate type of extrapolation depending on the order of the integrator used. In recent times the non exact character of the perturbative numerical solution of Eq. (8) has been debated. All in all, this is inherent in the nature of the perturbative expansion mechanism: the latter makes sense only provided an analytic solution exists, which is unavoidably lost in a process like an accept/reject mechanism. Obviously, many integration schemes can be adopted, whose relative merits have been discussed [3, 4]. In this work we considered the simplest possible choice, namely the Euler integrator. For further details and motivations the reader is referred to App. B.

1.2 Large deviations in NSPT simulations

Since the early times of NSPT it was clear that the ability to estimate perturbative coefficients using a stochastic method unavoidably exposes the results to statistical and systematic errors. We have already referred to errors coming from the numerical integration of the stochastic equation. Since we unavoidably have to work in finite volume, one should also care of finite volume effects. Certainly significant progress has been made with respect to both these [16, 6, 17, 3, 4]. On the other hand, the distributions of NSPT coefficients themselves reveal several features and peculiarities that must be handled with great care. This observation was triggered by some discrepancies between NSPT results and known ones for $O(3)$ non-linear sigma model ¹ and was subsequently investigated and characterized in detail for zero-dimensional models (in particular for the zero-dimensional $\lambda\phi^4$ model, the dipole random variable model and the Weingarten's "pathological model") [10]. The scenario that emerges is that, for all of them, the statistical properties of the process deviate significantly from those of a normal process, which exhibits exponentially suppressed tails. In contrast, NSPT stochastic processes at higher orders are characterized by long tails and rare events that introduce *spikes* that are difficult to handle with conventional statistical analysis. Despite the fact that estimating statistical errors can be done more safely adopting non-parametric methods (in particular the bootstrap method [10]), one is nevertheless left with the practical challenge of understanding if (and to which extent) one can get precise estimates at high perturbative orders for low-dimensional systems.

The possible appearance of large fluctuations at high orders is not surprising; looking at a simple model, even a simple-minded argument can provide a hint. Let us consider the zero-dimensional action:

$$S = \frac{1}{2}\varphi^2 + \frac{1}{3}g\varphi^3 \quad (9)$$

with the associated Langevin equation

$$\dot{\varphi} = -(\varphi + g\varphi^2) + \eta \quad (10)$$

Considering the perturbative expansion in Eq. (7) we obtain the following tower of equations:

$$\begin{aligned} \dot{\varphi}^{(0)} &= -\varphi^{(0)} + \eta \\ \dot{\varphi}^{(1)} &= -\varphi^{(1)} - \varphi^{(0)}\varphi^{(0)} \\ \dot{\varphi}^{(2)} &= -\varphi^{(2)} - 2\varphi^{(0)}\varphi^{(1)} \\ \dot{\varphi}^{(3)} &= -\varphi^{(3)} - (2\varphi^{(0)}\varphi^{(2)} + \varphi^{(1)}\varphi^{(1)}) \\ &\dots \end{aligned} \quad (11)$$

¹This observation was made by M. Pepe [18] and that's why the effect is often referred to as *Pepe effect*.

It is clear that any oscillation dictated by the Gaussian noise at the leading order propagates squared at the first order, results in a cubic effect at the third order and so on. All in all, a potentially large fluctuation is magnified at higher and higher perturbative orders, and we are naturally led to consider the possibility that this mechanism can ultimately make the signal a wild one. Will the restoring mechanism which is built into the Langevin equation be effective enough to reabsorb large fluctuations? How long will this mechanism take and what are the effects on the autocorrelation time of the process? Are we guaranteed that a finite standard deviation will emerge? These are examples of the questions that we naturally ask ourselves. A natural hypothesis is of course that this mechanism will be less and less severe when more degrees of freedom come into play (coherent large fluctuations will be unlikely and all in all the coupling of the many degrees of freedom are expected to eventually result in some - maybe slow - convergence to gaussianity). Of course, then again the question arises of how large a system should be to stay on a safe side.

This well-known problem has recently come back in the framework of NSPT computation of perturbative expansions around non-trivial vacua. This formulation of NSPT has to be considered a natural one (in the same spirit, there is work on the Schrödinger Functional [19, 20]) and would be very useful, given the intricate nature of standard perturbation theory in this context. Some preliminary steps have been taken, starting from low-dimensional models like the Double Well Potential [21]. Not surprisingly, fluctuations were back; actually they are the biggest hurdles in assessing the feasibility of these calculations.

1.3 A testing ground for a natural conjecture

The structure shown in Eq. (11) is quite general, but the fact that we can expect less problems for a large number of degrees of freedom is apparently confirmed by the case of Lattice QCD, where fluctuations do eventually take place at very high orders, but these are beyond those needed, for example, to inspect asymptotic behaviors. In large systems the order-by-order equations are coupled and, along the same simple lines as those pinned down in section 1.2, one expects that rare events affecting a single degree of freedom independently of the others will contribute less. All in all, it is natural to investigate the relations between NSPT stochastic distributions and the number of degrees of freedom. From this perspective, simulating $O(N)$ non-linear sigma models is a natural choice, as we can consider the same model for different values of the parameter N , changing the number of degrees of freedom. Certainly, having more and more degrees of freedom translates into a larger computational cost, so we have to prove we can get positive answers before too high computational costs are to be paid.

2 $O(N)$ non-linear sigma models

$O(N)$ non-linear sigma models provide a nice theoretical laboratory in quantum field theory. From a theoretical point of view, NLSM display properties that are crucial in understanding the dynamics of particles and fields, such as asymptotic freedom. From a phenomenological point of view, they have been able to model different features in different contexts (for an introduction to the model see *e.g* [22]). In the following we will not be concerned with any particular physical motivation, our interest for the model being motivated by the possibility to tune the parameter N , changing the number of degrees of freedom. In the continuum, we have the following action:

$$S = \frac{1}{2g} \int d\mathbf{x} \left(\partial_\mu \mathbf{s}(\mathbf{x}) \right)^2 \quad (12)$$

where $\mathbf{s}(\mathbf{x})$ is a N -component real scalar field constrained by $\mathbf{s}(\mathbf{x}) \cdot \mathbf{s}(\mathbf{x}) = 1$ for all \mathbf{x} (from now on, we will denote the point in space-time without bold). On the lattice, we can provide various discrete

versions of this theory. In this work we use the simplest $2D$ formulation, namely

$$S = -\frac{1}{g} \sum_{x,\mu} \mathbf{s}_x \cdot \mathbf{s}_{x+\mu} \quad \mathbf{s}_x \cdot \mathbf{s}_x = 1 \quad (13)$$

where \mathbf{s}_x is a N -component lattice real scalar field constrained by $\mathbf{s}_x \cdot \mathbf{s}_x = 1$ for all the lattice sites, g is the coupling constant and μ runs over the two lattice directions. The partition function of the system can be written by incorporating the constraint into a local Dirac delta function

$$Z = \int \prod_x d\mathbf{s}_x \delta(\mathbf{s}_x^2 - 1) e^{\frac{1}{g} \sum_{x,\mu} \mathbf{s}_x \cdot \mathbf{s}_{x+\mu}} \quad (14)$$

2.1 Perturbation theory

Perturbation theory requires correctly identifying the degrees of freedom. Following the standard approach [23], one way consists of eliminating the constraints by decomposing

$$\mathbf{s}_x = (\boldsymbol{\pi}_x, \sigma_x) \quad (15)$$

and rescaling

$$\boldsymbol{\pi}_x^2 \rightarrow g\boldsymbol{\pi}_x^2 \quad (16)$$

This way, we can integrate out the constraint in the partition function in Eq. (14), remaining only with the degrees of freedom associated with $\boldsymbol{\pi}_x$, which are now unconstrained. Neglecting insignificant terms in perturbation theory, we can write the partition function

$$Z = \lim_{\lambda \rightarrow 0} \int \prod_x d\boldsymbol{\pi}_x e^{-\frac{1}{2} \sum_{x,\mu} \left[(\Delta_\mu \boldsymbol{\pi}_x)^2 + \lambda^2 \boldsymbol{\pi}_x^2 - \frac{1}{g} (\Delta_\mu \sqrt{1 - g\boldsymbol{\pi}_x^2})^2 \right] - \frac{1}{2} \sum_x \log(1 - g\boldsymbol{\pi}_x^2)} \quad (17)$$

where Δ_μ is the usual lattice discretized version of the derivative; the logarithmic term arises from the additional integral measure term and λ is an infrared regulator, which needs to be removed at the end of the calculations. This latter term is required because the propagator is ill-defined in the infrared region, diverging as $\log \lambda$ (see [23]).

Perturbation theory, as usual, amounts to expanding the interaction terms in Eq. (17) in Taylor series and evaluating them on the free theory. This results in a highly intricate perturbation theory, where not only new Feynman diagrams are generated but also new vertices appear at each order [24]. In this work we consider a well-defined $O(N)$ invariant quantity ([23]), namely the energy (which is nothing but than the propagator in term of the original fields)

$$E = -\frac{1}{2V} \frac{\partial \log Z}{\partial \left(\frac{1}{g}\right)} = \langle \mathbf{s}_0 \cdot \mathbf{s}_1 \rangle = g \langle \boldsymbol{\pi}_0 \cdot \boldsymbol{\pi}_1 \rangle + \langle \sqrt{1 + g\boldsymbol{\pi}_0^2} \sqrt{1 + g\boldsymbol{\pi}_1^2} \rangle \quad (18)$$

(where a perturbative evaluation requires the Taylor series expansion of the square root).

2.2 NSPT setup for $O(N)$ NLSM

Calculating Eq. (18) in perturbation theory is a formidable task and up to now only the first four terms are known analitically [23, 24]. In the perturbative expression

$$E = E^{(0)} + gE^{(1)} + g^2E^{(2)} + g^3E^{(3)} + g^4E^{(4)} + \dots \quad (19)$$

the loop corrections read

$$\begin{aligned}
E^{(0)} &= 1 \\
E^{(1)} &= -(N-1)/4 \\
E^{(2)} &= -(N-1)/32 \\
E^{(3)} &= -0.00726994(N-1) - 0.00599298(N-1)^2 \\
E^{(4)} &= -0.00291780(N-1) - 0.00332878(N-1)^2 - 0.00156728(N-1)^3
\end{aligned} \tag{20}$$

With NSPT we can proceed straight ahead and go beyond the fourth order, especially (as already stated and as we will see) in the large N regime. In fact, NSPT simulations are completely insensitive to the increasing number of terms of the diagrammatic perturbation theory: the order-by-order encoding of Eq. (8) is naturally generated.

Eq. (17) can be rewritten as

$$\begin{aligned}
Z &= \int \prod_x d\pi_x \exp \left\{ \sum_{x,\mu} \left(\pi_x \cdot \pi_{x+\mu} + \frac{1}{g} \sqrt{1 - g\pi_x^2} \sqrt{1 - g\pi_{x+\mu}^2} \right) \right\} \\
&\quad \times \exp \left\{ -\frac{1}{2} \sum_x \log(1 - g\pi_x^2) \right\}
\end{aligned} \tag{21}$$

From the action

$$S = - \sum_{x,\mu} \left(\pi_x \cdot \pi_{x+\mu} + \frac{1}{g} \sqrt{1 - g\pi_x^2} \sqrt{1 - g\pi_{x+\mu}^2} \right) + \frac{1}{2} \sum_x \log(1 - g\pi_x^2) \tag{22}$$

it is straightforward to derive the associated Langevin equation

$$\dot{\pi}_y^j(\tau) = \sum_\mu \left\{ \pi_{y+\mu}^j + \pi_{y-\mu}^j - \pi_y^j \left(\sqrt{\frac{1 - g\pi_{y+\mu}^2}{1 - g\pi_y^2}} + \sqrt{\frac{1 - g\pi_{y-\mu}^2}{1 - g\pi_y^2}} \right) \right\} \bigg|_{\pi(\tau)} + \frac{g\pi_y^j}{1 - g\pi_y^2} \bigg|_{\pi(\tau)} + \eta_y^j(\tau) \tag{23}$$

$\pi_y^j(\tau)$ represents the j -component of the π field at the lattice site y , evaluated at the stochastic time τ . In the Euler scheme, the equation reads

$$\begin{aligned}
\pi_y^j(\tau + \Delta\tau) &= \pi_y^j(\tau) + \Delta\tau \sum_\mu \left\{ \pi_{y+\mu}^j(\tau) + \pi_{y-\mu}^j(\tau) \right. \\
&\quad \left. - \pi_y^j \left(\sqrt{\frac{1 - g\pi_{y+\mu}^2}{1 - g\pi_y^2}} + \sqrt{\frac{1 - g\pi_{y-\mu}^2}{1 - g\pi_y^2}} \right) \right\} \bigg|_{\pi(\tau)} + \Delta\tau \frac{g\pi_y^j}{1 - g\pi_y^2} \bigg|_{\pi(\tau)} + \sqrt{2\Delta\tau} \eta_y^j(\tau)
\end{aligned} \tag{24}$$

The Gaussian white noise is distributed according to a normal distribution with zero mean and unit variance (and now no Dirac delta is around). Again, after Eq. (7) has come into play at a given fixed-order, Eq. (24) gets translated into a tower of (perturbative) equations.

In Eq. (21), (22), (23) and (24) we consider directly the limit $\lambda \rightarrow 0$ so that the stochastic evolution exhibits a zero-mode that must be regularized. We have opted for the simplest scheme, *i.e.* a step-by-step subtraction of the zero-mode (see App. A for a discussion).

3 Fluctuations: how they show up and how they are tamed in the large N limit

We performed different simulations for several values of N on a 20×20 lattice, unless otherwise specified (see Tab. 1 for further details). Even on such a small lattice size we found tiny finite volume

| N | n_{max} | V | Statistics $\times N$ | $\Delta\tau$ |
|-------------|-----------|----------------|--------------------------|---|
| 5 : 1 : 15 | 15 | 20×20 | $\approx 1.6 \cdot 10^9$ | $[18, 25, 35, 50, 75, 100] \cdot 10^{-4}$ |
| 18 : 3 : 45 | 15 | 20×20 | $\approx 2.1 \cdot 10^9$ | $[18, 25, 35, 50, 75, 100] \cdot 10^{-4}$ |
| 15 : 3 : 43 | 23 | 20×20 | $\approx 1.2 \cdot 10^9$ | $[18, 25, 35, 50, 75, 100] \cdot 10^{-4}$ |
| 45 | 23 | 20×20 | $\approx 2.7 \cdot 10^9$ | $[18, 25, 35, 50, 75, 100] \cdot 10^{-4}$ |
| 5 | 23 | 66×66 | $\approx 9 \cdot 10^7$ | $[18, 25, 35, 50, 75, 100] \cdot 10^{-4}$ |

Table 1: Simulation details. The notation $N_1 : m : N_2$ stands for $N_1, N_1 + m, N_1 + 2m, \dots, N_2$. 6 different time step sizes $\Delta\tau$ were considered. n_{max} indicates the highest perturbative order in a given set of simulations; notice that streams with different n_{max} have to be considered separately because of correlations among the different orders in a given stream. Statistics is normalized by N , *i.e.* different rows have approximately the same computational weight.

effects as far as the first four known values are concerned (see Eq. (20) [24]): discrepancies are of the order of a few per mille. In Fig. 2 we plot NSPT predictions and exact results. Systematic effects coming from the choice of the numerical integration scheme in Eq. (24) have been removed. Details about extrapolations (which asks for dealing with the minimization of a χ^2 and the estimation of autocorrelations) are discussed in App. B and App. C.

Having looked at Fig. 2, the reader is invited to look back at Fig. 1, where one can easily grasp the effect of N on the maximum perturbative order we could compute. The difference between the low and the high perturbative order (n) regions is evident: for all the values of $N \geq 5$ which are taken into account, we could compute three extra orders on top of the ones that were already known, but as n increases, we were able to obtain reliable results only for increasing N . More precisely, for the $O(5)$ NLSM model we pushed the calculation from the fourth up to the seventh order, for $O(15)$ we reached the tenth order, and for $O(45)$ even the 14th order was calculated. As already said, this is related to the fluctuations in the stochastic process, in a way that will be evident in the figures that we are going to display in the following. It is not trivial to determine at which perturbative order n one will have to stop for a given $O(N)$ NLSM model. In the following we will provide at least a few sanity checks by looking at time series, cumulative moving averages and standard deviations and (later on) scaling of (estimations of) relative errors.

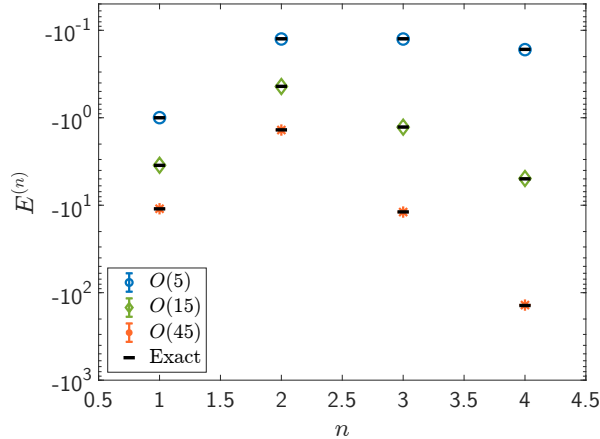


Figure 2: NSPT computations of the energy for $O(5)$ (blue markers), $O(15)$ (green markers) and $O(45)$ (orange markers) up to the fourth order; analytical values are plotted in black. The errorbars are not visible as they are smaller than the markers. Computations were performed on a 20×20 lattice.

The fact that large fluctuations show up is evident by inspection of Fig. 3, where we display the signals (*i.e.* stochastic time series) of NSPT simulations for $O(5)$, $O(15)$ and $O(45)$ (same color code

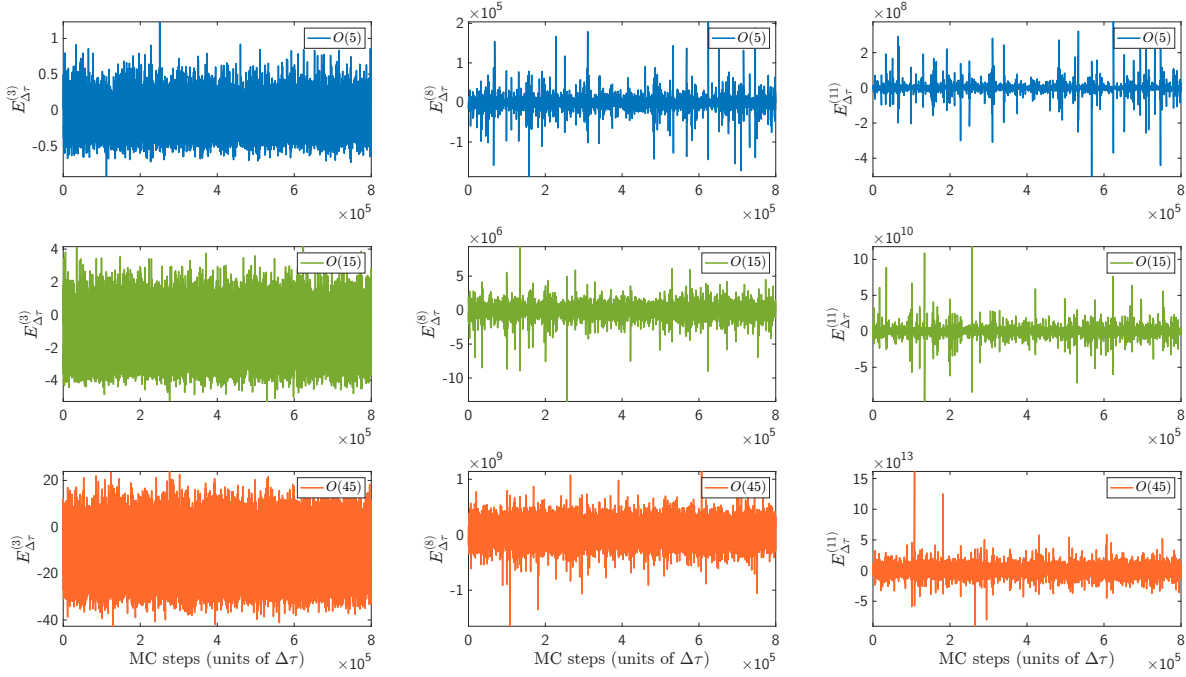


Figure 3: NSPT signals for the $O(5)$ (blue lines), $O(15)$ (green lines) and $O(45)$ (orange lines) models at $\Delta\tau = 0.0035$ for $n = 3$ (left), $n = 8$ (center) and $n = 11$ (right). We considered for all models 800000 steps, after having previously subtracted 4000 thermalization steps (a number chosen looking at the highest order).

as in Fig. 1): comparison is made at the same value of $\Delta\tau = 0.0035$. In the first column, we show the evolution in stochastic time of the signals at $n = 3$: no sign of large fluctuations is there. By studying the distribution of the signals, one finds that these are (very) similar to a Gaussian process, not exhibiting long tails. Most importantly, no significant differences are there for different values of N . This is no longer true at perturbative order $n = 8$ (second column): large spikes emerge for the $O(5)$ model which contribute significantly to the mean and standard deviation of the distribution (in section 3.1 we report a more complete characterization). On the other hand, the signal for $O(15)$ still seems manageable, and that for $N = 45$ looks excellent. Notice that most of the fluctuations (at any value of n and N) are distributed within what looks like a *band*: if we want to inspect the presence of large fluctuations by eye, we have to compare them to the width of this band. An even more extreme situation shows up in the last column (perturbative order $n = 11$). For $N = 5, 15$ we inspect large fluctuations, which result in significant deviations from the gaussian distribution and in a signal which appears bad in terms of signal to noise ratio. On the other hand, the stochastic time history for $N = 45$ (last row) appears under control (remember: we have to compare the size of fluctuations to the width of the band in which most of them fall); we felt comfortable with the distributions.

3.1 Cumulative moving averages and standard deviations

Cumulative moving average and standard deviation are statistical tools that can be helpful in analysing our data: we take them into account in the same spirit as in [10]. Roughly speaking, the cumulative (moving) counterparts of mean and standard deviation evolve as more data points are added and track how data spread out as new observations are considered. This is a most natural way of assessing data stability with respect to the occurrence of (large) fluctuations. We define the cumulative moving

average (in short, cumulative mean) as

$$\langle E^{(n)} \rangle_\tau = \frac{1}{\tau} \sum_{i=1}^{\tau} E_i^{(n)} \quad (25)$$

where $E_i^{(n)}$ stands for the n -th perturbative order of the energy measured on the i -th Monte Carlo configuration (as it is easily seen, we make use of the same wording as for standard, non-perturbative Monte Carlo simulations; keep in mind that here a configuration is a collection of values of the field at different orders, at a given stochastic time). The subscript $\langle \dots \rangle_\tau$ indicates that the averaging window extends from the first configuration to the τ -th. Similarly, we can define the cumulative standard deviation

$$\sigma(E^{(n)})_\tau = \sqrt{\langle E^{(n)2} \rangle_\tau - \langle E^{(n)} \rangle_\tau^2} \quad (26)$$

A good Monte Carlo simulation, accurately exploring a well-defined distribution, should exhibit for $\tau \gg 1$ an approximately constant (asymptotic) value for the quantities in Eq. (25) and (26). To make a fair comparison between results obtained at various values of N , which are expected to span different orders of magnitude (see Fig. 1), it is a good idea to focus on relative fluctuations with respect to the estimated mean. This motivated our choice of how to plot Fig. 4 and Fig. 5: y -value ranges have been chosen as $[\hat{y} - \delta\hat{y}, \hat{y} + \delta\hat{y}]$, where \hat{y} is the best estimation of the quantity at hand and $\delta\hat{y}$ is the spread amounting to a given percentage variation (which is the same, at a given order, for all the signals that we compare). Additionally, larger values of N are computationally more expensive to simulate but are expected to result in better self-averaging effects, so that we decided to compare different Monte Carlo histories at the same computational time rather than at the same statistics. The cumulative means and standard deviations that we display have been obtained by time histories at the same value of $\Delta\tau = 0.01$ (the effect is roughly the same at different values of $\Delta\tau$; this should appear clear by looking back at Fig. 3, where the same overall picture emerged from comparisons made with the different choice of $\Delta\tau = 0.0035$).

The scenario that emerges for the quantity defined in Eq. (25) is consistent with what was broadly seen before, as it can be seen from Fig. 4. The latter is organised exactly as Fig. 3: on a given column, the perturbative order is fixed (as before, $n = 3, n = 8, n = 11$), while N stays the same on a given row (as before, $N = 5, N = 15, N = 45$). At a low perturbative order (first column, $n = 3$), at any value of N the cumulative means are seen to flatten, as we would expect them to do. On the contrary, the picture changes dramatically as the loop order increases. In the middle column ($n = 8$) the cumulative mean for $O(5)$ does not flatten that well; it is subject to significant fluctuations and even with a substantial amount of statistics we are not sure we are getting a reliable estimate of the mean). It does not take too long for the signal for $O(15)$ to display a similar effect: see the last column ($n = 11$). For $O(45)$ the cumulative mean can be considered stable and, since this observation is independent of $\Delta\tau$, a subsequent $\Delta\tau \rightarrow 0$ extrapolation turns out to be well under control.

For smaller values of N the scenario is even worse when analyzing the standard deviation (see Fig. 5, which is plotted with the same conventions as in Fig. 4). Obviously, due to the definition of the standard deviation, any fluctuation gives only positive contributions. All in all, for $N = 5, n \geq 8$ and $N = 15, n \geq 11$ we cannot be sure that our estimations of the variance are reliable. However, in this case as well, we can inspect well flattening signals for large enough N . Actually, for $O(45)$ we could not detect pathological effects up to $n = 14$. As another sanity check, we verified that for $N = 45$ the statistical errors are observed to scale correctly as $\sim \frac{1}{\sqrt{N_{samples}}}$.

All in all, we have clear hints that for given values of N our best estimations of mean and standard deviation could be unreliable. We will see that these findings are confirmed and a more clear description appears by looking at the scaling of (best estimations of) relative errors: we present this analysis in section 4.

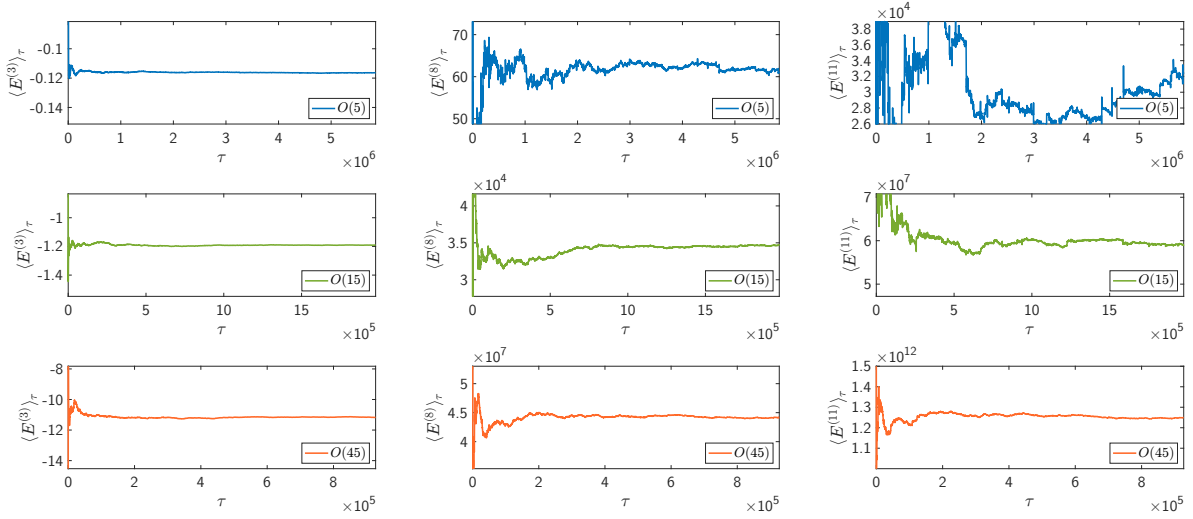


Figure 4: Time evolution of the mean (cumulative moving averages) for $O(5)$ (blue lines), $O(15)$ (green lines) and $O(45)$ (orange lines). In all cases, $\Delta\tau = 0.01$. Comparisons are made at equal computational time, i.e. with $N_{stat} \cdot N_{dof} \sim \text{const}$ (N_{stat} being the number of time steps). y -value ranges have been chosen as $[\hat{y} - \delta\hat{y}, \hat{y} + \delta\hat{y}]$, where \hat{y} is the best estimation of the quantity at hand and $\delta\hat{y}$ is a spread amounting to a given percentage variation (which is the same, at each perturbative order, for all the signals that we compare).

3.2 Large volumes and large N

A key concept for the reliability of a lattice Monte Carlo simulation is the property of lattice self-averaging: for a given theory, as the size of the lattice grows, one has to observe more stable statistical averages. We expect that using larger and larger lattices for computations of local quantities (as in Eq. (18)) results in a reduction of the standard deviation. On the other hand, we have just seen that, at a given NSPT order, fluctuations are tamed with increasing N (i.e. with increasing number of local degrees of freedom). Naively, one could ask to which extent the two effects are related: not surprisingly, we will see that these two effects are fundamentally different.

In this regard, we can inquire about the *true* size of the system (and inspect the effects on what we could broadly think of as NSPT self-averaging properties). Naively, one could think of considering the same total number of degrees of freedom (namely, we can compare the large N - small L regime with the small N - large L regime). In the left plot of Fig. 6 we inspect the expected self-averaging effect for $O(5)$. Namely, we compare stochastic time histories (stochastic time series) at $n = 1$ order on $L^2 = 66 \times 66$ and $L^2 = 20 \times 20$: as expected, considering a larger lattice results in less statistical fluctuations. In the right plot of Fig. 6 we consider a much higher order, namely $n = 13$. Here we compare NSPT results for $O(5)$ on a lattice volume $L^2 = 66 \times 66$ with NSPT results for $O(45)$ on $L^2 = 20 \times 20$: in this comparison the overall number of degrees of freedom is (roughly) the same. Given the polynomial dependence in N (see Eq. (20) at order $n = 1, 2, 3, 4$), we expect the two signals (for $O(5)$ and $O(45)$) to differ significantly in orders of magnitude: to compare them we need to normalize the data. We decided to look at cumulative means normalized to our best estimates. In practice, at each stochastic time we divide the cumulative means by the mean value calculated over the entire sample (we denote with a bar the quantities normalized in this way: $\langle \bar{E}^{(n)} \rangle_\tau$). It is evident that the small L - large N combination does not help that much for computing high perturbative orders: taming large deviations appears to be a genuine large N effect.

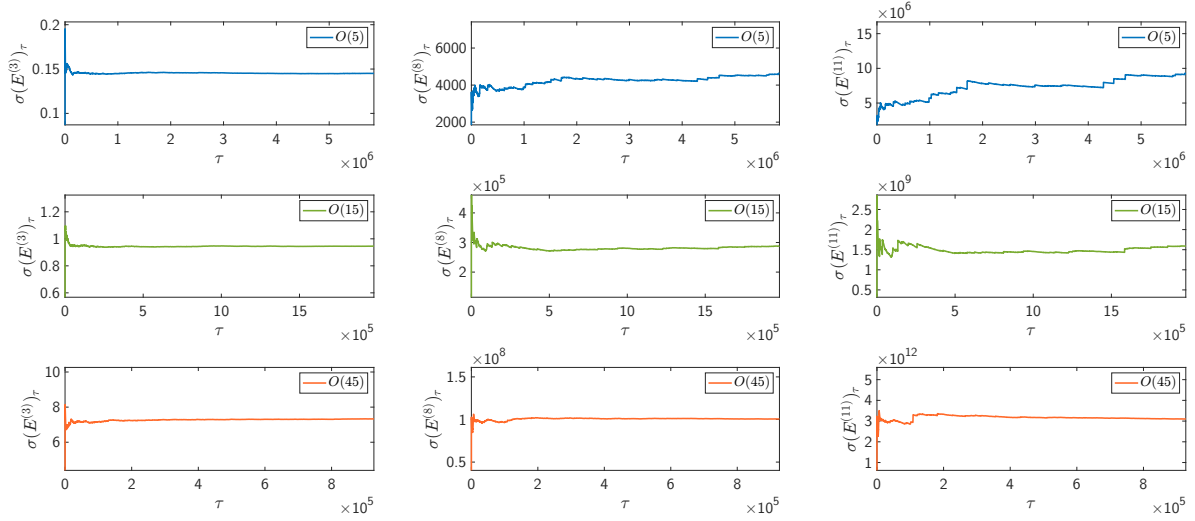


Figure 5: Time evolution of the standard deviation (cumulative moving standard deviation) for $O(5)$, $O(15)$ and $O(45)$; $\Delta\tau = 0.01$. Same plotting conventions as in Fig. 4.

4 Probing NSPT fluctuations with relative errors

In Monte Carlo simulations, studying relative errors scaling is very useful for assessing the robustness of the results; of course NSPT is no exception. In this section, we make use of very general assumptions about the behavior of relative errors as functions of the two parameters N and n . Through this analysis, we show how to identify *a posteriori* N regions where NSPT results appear to be reliable and regions where the accuracy is lost: all in all, we want once again to assess the meaning of *large* N for a NSPT computation of a $O(N)$ quantity at a given perturbative order n .

4.1 n-scaling

From now on, we denote relative errors as

$$\Delta_N^{(n)} = \left. \frac{\delta E^{(n)}}{E^{(n)}} \right|_N \quad (27)$$

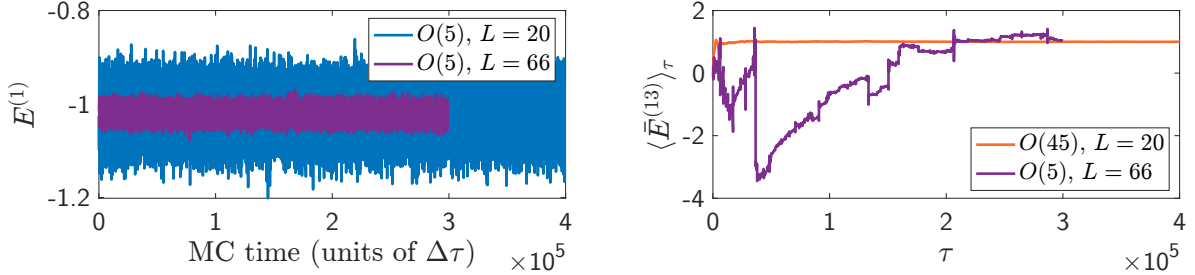


Figure 6: Left plot: $O(5)$ model at the lowest, $n = 1$ perturbative order for different lattice sizes ($L^2 = 66 \times 66$ and $L^2 = 20 \times 20$). Right plot: a comparison between the cumulative averages of the the $n = 13$ perturbative order for $O(5)$ on a 66×66 lattice and $O(45)$ on a 20×20 lattice. The two models have (roughly) the same total number of degrees of freedom.

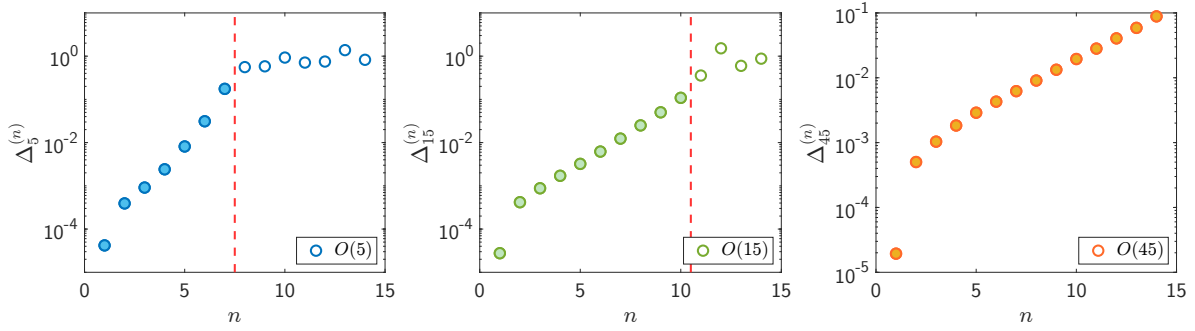


Figure 7: Evaluation of the relative error in Eq. 27 as a function of loop order for $O(5)$, $O(15)$ and $O(45)$. The solid markers indicate the results that we could regard as safe: the red dashed line separates safe and unsafe regions. Thresholds are the same as those guessed from the analysis of cumulative means and standard deviations.

For a given $O(N)$ we study the ratio of the value of the energy at the n -th perturbative order $E^{(n)}$ and the associated error $\delta E^{(n)}$. Notice that both are coming from the stochastic time extrapolation procedure that we describe in App. B and C. In particular, they are supposed to contain all the information regarding auto-correlations and cross-correlations. We stress that we compute the ratio in Eq. (27) (and later on in Eq. (28)) out of our *best estimations* of $E^{(n)}$ and $\delta E^{(n)}$. Since we have already seen that problems are around at high orders, we must be ready to accept that we did our best, but some of these estimations will be unreliable; as a matter of fact, this is what will happen. First of all, we will analyze the quantity in Eq. (27) as a function of the integer parameter n for fixed values of N .

A natural general hypothesis is that relative errors should be monotonically increasing in n : all in all, we have already seen that higher-order computations result in progressively larger standard deviations as n increases. Part of this will also come from non-trivial effects of cross-correlations as a function of n (a given order of the field depends on all the fields at lower order as indicated in Eq. (8)).

In Fig. 7 we plot $\Delta_N^{(n)}$ as a function of n for various values of N : the three panels once again refer to $O(5)$, $O(15)$ and $O(45)$. As far as one sees a smooth behavior, one inspects an exponential growth. Notice that up to $n = 14$ for $O(45)$ we observe no violations of our hypothesis: relative errors are monotonically increasing. The same does not hold for lower values of N , in particular for $n > 7$ in the $O(5)$ case and for $n > 10$ in the $O(15)$ case. These thresholds seem to be in agreement with what has been discussed in section 3.1 and are yet another reason for plotting Fig. 3. We have already made the point that we have been working with *best estimations* and we ended up with having to give up with some of them. As an extra piece of information, notice that we had also found less smooth continuum stochastic time extrapolations for the perturbative orders which turned out to be unreliable.

4.2 N -scaling

It appears natural to look also for an N -scaling analysis of relative errors. Consider the quantity

$$\bar{\Delta}_N^{(n)} = \left. \frac{\delta E^{(n)}}{E^{(n)}} \right|_N \cdot \Gamma(N) \quad (28)$$

The definition is the same as before, apart for the presence of the factor $\Gamma(N)$. This has to be understood as follows. Different values of N result in higher and higher computational efforts, but also in different values of autocorrelations and cross-correlations. Once we have taken into account all the data that are available for each value of N , the factor $\Gamma(N)$ is in charge of correcting for different statistics: in other words, we compare relative errors for different N at the same statistics in terms of independent measures taken.

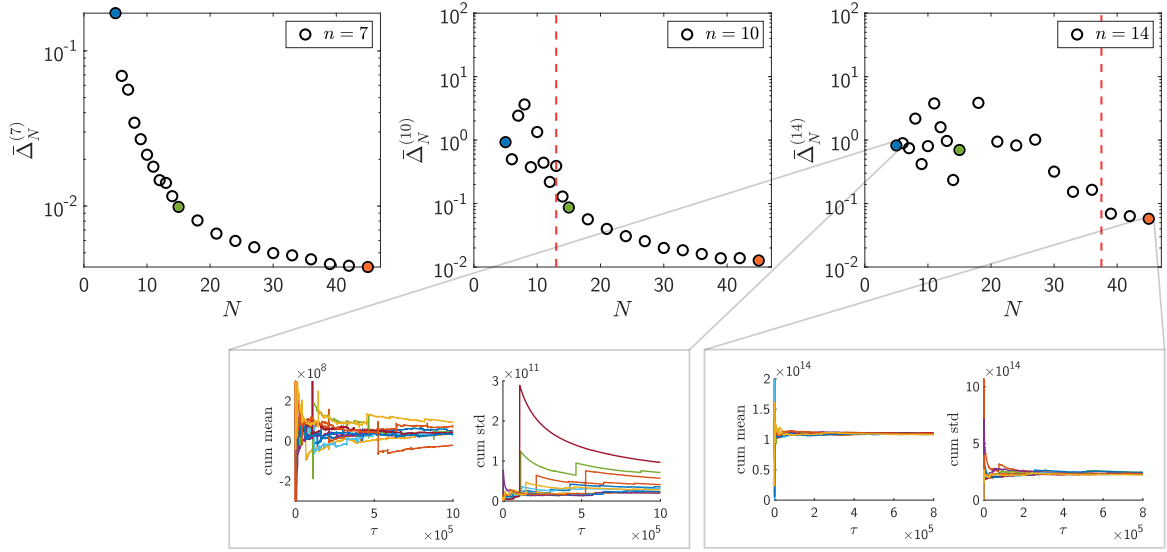


Figure 8: Scaling of the relative errors defined in Eq. (28) as a function of the integer parameter N for all the models (from $O(5)$ to $O(45)$) listed in Tab. 1; the three plots refer to perturbative orders $n = 7, 10, 14$. The filled points refer to $O(5)$, $O(15)$, and $O(45)$ (same color code as before, in particular as in Fig. 1). The red dashed line separates the regions where we inspect the expected scaling from the regions where we see violations. To make contact with what has already been shown, in the small panels we show cumulative means and standard deviations for 10 different independent runs for $O(5)$ and $O(45)$ at the 14-th perturbative order.

On very general grounds we claim that the quantity in Eq. (28) must exhibit a monotonically decreasing behavior in N (all in all, after taking the factor $\Gamma(N)$ into account, we are left with different numbers of degrees of freedom depending on N). This is perfectly observed at small values of n , in particular for $n \leq 7$: see for $n = 7$ the left plot of Fig. 8 ($O(5)$, $O(15)$ and $O(45)$ results are highlighted with the same color code we have been using till now). For $n = 10$ (central panel), the expected monotonic behavior only sets in for $N > 12$, while for $n = 14$ we need to look at the very largest values of N to inspect the expected behavior.

All in all, we have been looking at different indicators in order to inspect what value of N is large enough for a given perturbative order n . We want to stress that, whatever indicator we considered, we have always found the same answer. To further stress this, the reader is invited to have a look at the right panel ($n = 14$) of Fig. 8. $O(5)$ and $O(45)$ results sit in different regions: only $O(45)$ results are candidate as reliable. Now look at the small panels. To make contact to what we have already looked at, we plot cumulative means and standard deviations for the energy at perturbative order $n = 14$ for $O(5)$ and $O(45)$ as obtained from several independent simulations: the difference is impressive.

5 Conclusions and prospects

We made use of NSPT to compute the energy of $O(N)$ Non Linear Sigma Models, for several increasing values of N . Our first goal was to establish that indeed for relatively *small* number of degrees of freedom we would find increasing large fluctuations for NSPT computations at increasing perturbative orders n , actually so large that at some point the signal to noise ratio is not under control. At the same time, we were able to verify a simple conjecture: NSPT high order computations are expected to be safe when we deal with a *large* number of degrees of freedom. Our main conclusion is that high orders

fluctuations are tamed for *large* N : basically, the larger is N , the larger is the perturbative order n that we can safely compute. While there is still (admittedly) a lack of fundamental understanding, we found that *a posteriori* it was possible to state how large N must be to safely compute at perturbative order n . Different indicators for the selection of such thresholds result in the same conclusions. It will be interesting to compare our results with large N results obtained by standard continuum techniques [25, 26, 27].

Once we have found that NSPT computations can be safely performed for large enough N , we have the chance to inspect asymptotics, in particular the expected IR-renormalon behavior. This is what we are doing in [28] (fully accounting for finite volumes effects). The present work has been in part motivated by problems encountered in NSPT computations around non trivial vacua (double well potential in Quantum Mechanics [21]). The idea is now to go for non-trivial vacua NSPT computations in $CP(N-1)$ models, which were among the very first related to resurgence scenarios [29].

Acknowledgments

We thank Petros Dimopoulos for very interesting discussions. This work was supported by the European Union Horizon 2020 research and innovation programme under the Marie Skłodowska-Curie grant agreement No 813942 (EuroPLEx) and by the INFN under the research project (*iniziativa specifica*) QCCLAT. This research benefits from the HPC (High Performance Computing) facility of the University of Parma, Italy.

References

- [1] F. Di Renzo et al. Four-loop result in $SU(3)$ lattice gauge theory by a stochastic method: lattice correction to the condensate. In: *Nuclear Physics B* 426.3 (Sept. 1994), pp. 675–685.
- [2] G. Parisi and Yong-shi Wu. Perturbation Theory Without Gauge Fixing. In: *Sci. Sin.* 24 (1981), p. 483.
- [3] Mattia Dalla Brida, Marco Garofalo, and A.D. Kennedy. Investigation of new methods for numerical stochastic perturbation theory in φ^4 theory. In: *Physical Review D* 96.5 (Sept. 2017).
- [4] Mattia Dalla Brida and Martin Lüscher. SMD-based numerical stochastic perturbation theory. In: *The European Physical Journal C* 77.5 (May 2017).
- [5] F. Di Renzo et al. High-loop perturbative renormalization constants for Lattice QCD. I. Finite constants for Wilson quark currents. In: *Eur. Phys. J. C* 51 (2007), pp. 645–657. arXiv: [hep-lat/0611013](#).
- [6] Gunnar S. Bali et al. Perturbative expansion of the energy of static sources at large orders in four-dimensional $SU(3)$ gauge theory. In: *Physical Review D* 87.9 (May 2013).
- [7] L. Del Debbio, F. Di Renzo, and G. Filaci. Large-order NSPT for lattice gauge theories with fermions: the plaquette in massless QCD. In: *The European Physical Journal C* 78.11 (Nov. 2018).
- [8] F. Di Renzo and L. Scorzato. Numerical Stochastic Perturbation Theory for full QCD. In: *Journal of High Energy Physics* 2004.10 (Oct. 2004), pp. 073–073.
- [9] Guilherme Catumba, Alberto Ramos, and Bryan Zaldivar. *Stochastic automatic differentiation for Monte Carlo processes*. 2023.
- [10] R. Alfieri et al. Understanding stochastic perturbation theory: toy models and statistical analysis. In: *Nuclear Physics B* 578.1-2 (July 2000), pp. 383–401.
- [11] Antonio González-Arroyo et al. Numerical stochastic perturbation theory applied to the twisted Eguchi-Kawai model. In: *Journal of High Energy Physics* 2019.6 (June 2019).

- [12] Poul H. Damgaard and Helmuth Hüffel. Stochastic quantization. In: *Physics Reports* 152.5-6 (Aug. 1987), pp. 227–398.
- [13] A. Ukawa and M. Fukugita. Langevin Simulation Including Dynamical Quark Loops. In: *Physical Review Letters* 55.18 (Oct. 1985), pp. 1854–1857. ISSN: 0031-9007.
- [14] G. G. Batrouni et al. Langevin simulations of lattice field theories. In: *Physical Review D* 32.10 (Nov. 1985), pp. 2736–2747. ISSN: 0556-2821.
- [15] Gareth O. Roberts and Jeffrey S. Rosenthal. Optimal Scaling of Discrete Approximations to Langevin Diffusions. In: *Journal of the Royal Statistical Society Series B: Statistical Methodology* 60.1 (Jan. 1998), pp. 255–268. ISSN: 1467-9868.
- [16] M. Brambilla and F. Di Renzo. High-loop perturbative renormalization constants for Lattice QCD (II): three-loop quark currents for tree-level Symanzik improved gauge action and $n_f=2$ Wilson fermions. In: *Eur. Phys. J. C* 73.12 (2013), p. 2666. arXiv: 1310.4981 [hep-lat].
- [17] Gunnar S. Bali, Clemens Bauer, and Antonio Pineda. Perturbative expansion of the plaquette to $\mathcal{O}(\alpha^{35})$ in four-dimensional SU(3) gauge theory. In: *Physical Review D* 89.5 (Mar. 2014).
- [18] Michele Pepe. MA thesis. University of Milano, 1996.
- [19] Christian Torrero and Gunnar S. Bali. NSPT calculations in the Schrödinger Functional formalism. In: *Proceedings of The XXVII International Symposium on Lattice Field Theory — PoS(LAT2009)*. LAT2009. Sissa Medialab, June 2010.
- [20] Dirk Hesse et al. The Schrödinger Functional in Numerical Stochastic Perturbation Theory. In: *Proceedings of 31st International Symposium on Lattice Field Theory — PoS(LAT2013)*. LATTICE 2013. Sissa Medialab, Apr. 2014.
- [21] Paolo Baglioni and Francesco Di Renzo. Numerical Stochastic Perturbation Theory around instantons. In: *Proceedings of The 39th International Symposium on Lattice Field Theory — PoS(LAT2022)*. LATTICE2022. Sissa Medialab, Jan. 2023.
- [22] Jean Zinn-Justin. Quantum Field Theory and Critical Phenomena. Oxford University Press, June 2002. ISBN: 9780198509233.
- [23] Shmuel Elitzur. The applicability of perturbation expansion to two-dimensional goldstone systems. In: *Nuclear Physics B* 212.3 (Feb. 1983), pp. 501–518. ISSN: 0550-3213.
- [24] B. Allés, A. Buonanno, and G. Cella. Perturbation theory predictions and Monte Carlo simulations for the 2D $O(n)$ non-linear σ -models. In: *Nuclear Physics B* 500.1–3 (Sept. 1997), pp. 513–543. ISSN: 0550-3213.
- [25] E. Brézin and J. Zinn-Justin. Renormalization of the Nonlinear σ in $2+\varepsilon$ Dimensions—Application to the Heisenberg Ferromagnets. In: *Physical Review Letters* 36.13 (Mar. 1976), pp. 691–694. ISSN: 0031-9007.
- [26] E. Brézin and J. Zinn-Justin. Spontaneous breakdown of continuous symmetries near two dimensions. In: *Physical Review B* 14.7 (Oct. 1976), pp. 3110–3120. ISSN: 0556-2805.
- [27] William A. Bardeen, Benjamin W. Lee, and Robert E. Shrock. Phase transition in the nonlinear σ in a $(2 + \varepsilon)$ -dimensional continuum. In: *Physical Review D* 14.4 (Aug. 1976), pp. 985–1005. ISSN: 0556-2821.
- [28] Paolo Baglioni and Francesco Di Renzo. Large order computations in $O(N)$ non-linear sigma models: renormalons, finite size effects and all that (in preparation). 2024.
- [29] Gerald V. Dunne and Mithat Unsal. Resurgence and Trans-series in Quantum Field Theory: The CP(N-1) Model. In: *JHEP* 11 (2012), p. 170. arXiv: 1210.2423 [hep-th].
- [30] Christof Gattringer and Christian B. Lang. Quantum Chromodynamics on the Lattice: An Introductory Presentation. Springer Berlin Heidelberg, 2010. ISBN: 9783642018503.

- [31] Ulli Wolff. Monte Carlo errors with less errors. In: *Computer Physics Communications* 156.2 (Jan. 2004), pp. 143–153. issn: 0010-4655.
- [32] Alberto Ramos. Automatic differentiation for error analysis of Monte Carlo data. In: *Computer Physics Communications* 238 (May 2019), pp. 19–35. issn: 0010-4655.
- [33] Fabian Joswig et al. pyerrors: A python framework for error analysis of Monte Carlo data. In: *Computer Physics Communications* 288 (July 2023), p. 108750. issn: 0010-4655.

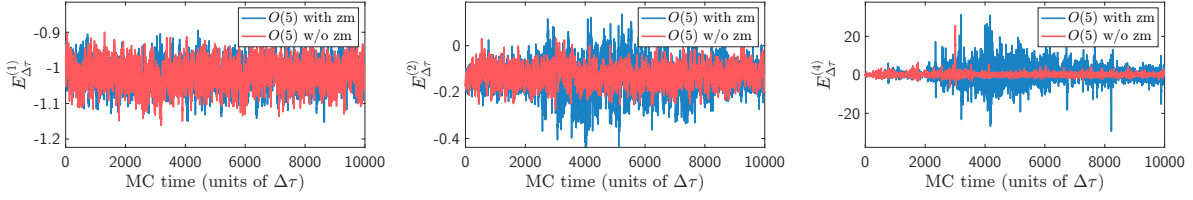


Figure 9: NSPT time series for the energy of $O(5)$ NLSM model (20×20 lattice). Different panels represent increasing loop orders, with (blue lines) and without (red lines) subtraction of zero-mode. The expected on average cancelation of divergence is taking place, but (as expected) one pays a huge noise price.

Appendix A: Zero-mode regularization

Given the action in Eq. (22), it is straightforward to verify that the basic building block of the diagrammatic perturbation theory, the propagator

$$\langle \pi_x \cdot \pi_y \rangle = \sum_{y,k} \delta_{yk} \langle \pi_x^y \pi_y^k \rangle \quad (29)$$

is ill-defined, having a zero-mode. An interesting feature is that if we consider only $O(N)$ invariant quantities, like the complete propagators

$$\langle \mathbf{s}_x \cdot \mathbf{s}_y \rangle = g \langle \pi_x \cdot \pi_y \rangle + \langle \sigma_x \sigma_y \rangle \quad (30)$$

these are well-defined quantities because the last term in Eq. (30) cancel order-by-order the zero-mode contribution [23]. From the NSPT point of view, this cancellation is expected to take place on average, which means plagued by statistical noise. One possibility is to introduce an infrared regulator λ in the same spirit of Eq. (17) and to remove it via a $\lambda \rightarrow 0$ extrapolation. This results in additional computational load. Moreover, in our experience, to achieve good numerical signals one has to live with quite large values of λ . A simpler and more effective choice is to remove the zero mode order-by-order, subtracting this contribution directly from the field (a recipe also used for LGT [8]). This procedure is very cheap and in principle correct in the thermodynamic limit, while at finite volume it introduces extra finite size effects. As seen, these are nevertheless tested to be small (almost negligible up to the fourth loop order). Subtraction of zero mode and on average subtraction are compared in Fig. 9 for the $O(5)$ model.

Appendix B: $\Delta\tau \rightarrow 0$ extrapolations

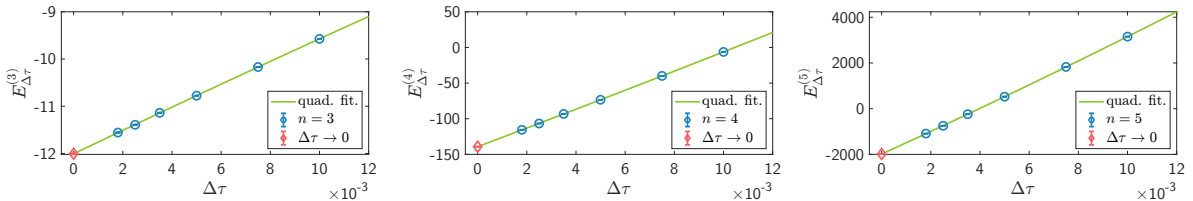


Figure 10: Example of $\Delta\tau \rightarrow 0$ extrapolation in the $O(15)$ model for perturbative order $n = 3, 4, 5$ (on a 20×20 lattice); we obtain $\chi_{red.}^2 \approx 1.33$. Blue markers represent measurements at different stochastic time step (notice that errors are too small to be seen), green lines are the quadratic fit estimated by means of Eq. 31 and red diamonds are the extrapolated quantities.

Coefficients of different perturbative orders in an NSPT computation at a given $\Delta\tau$ are correlated, while at different $\Delta\tau$ values of course they are not. In force of that, the extrapolation to vanishing stochastic time step (see Fig. 10) has been performed minimizing the generalised χ^2 function [7]:

$$\chi^2 = \sum_{n,m,\Delta\tau} (E_{\Delta\tau}^{(n)} - \alpha_n \Delta\tau - \beta_n \Delta\tau^2 - E^{(n)}) \Sigma_{\Delta\tau}^{-1}(n,m) (E_{\Delta\tau}^{(m)} - \alpha_m \Delta\tau - \beta_m \Delta\tau^2 - E^{(m)}) \quad (31)$$

where it can be seen that both linear and quadratic effects in the time step can be (and have been) considered in the extrapolation. The indexes run on perturbative orders $n, m \in [0, 1, \dots, n_{max}]$, being n_{max} the maximum perturbative order included in the fit. $\Sigma_{\Delta\tau}^{-1}(n, m)$ is the inverse of the covariance matrix at the same $\Delta\tau$ encoding the correlation between different perturbative orders n and m . $E^{(n)}$ are the extrapolated quantities we are interested in. The block diagonal $\Sigma_{\Delta\tau}^{-1}(n, m)$ matrix encodes also the cross- and auto-correlations (see App. C for a detailed discussion). In addition the Gaussian Sampling method was used for error propagation.

The fact that we have to live with an extrapolation in the stochastic time has been quite debated. All in all, we are here making use of the simplest recipe, namely the Euler scheme. Other schemes are viable, which we also make use of (see the following). A key point is that we are here interested in high orders, so we want to make sure that extrapolation is safe, taking every perturbative order into account. One temptation to stay away from is that of thinking that for some higher order scheme a single value of the time step can be relied on. There is no way of getting a value of the time step which is *small enough* to ensure a precision which we cannot distinguish from statistical errors: higher orders can always hold surprises (and in general they do, at least because orders of magnitude can be very different at different orders). As an extra comment, notice that a stochastic time etrapolation turning out to be viable is yet another indication that a result at a given order is safe (from the point of view of huge fluctuations). In other words, stochastic time extrapolation does result in computational efforts, but it can make us more confident we can trust means and errors we compute at fixed values of $\Delta\tau$. This is in the end the main thing we are interested in here.

There are cases in which we actually do even more, that is we even make use of more than one numerical scheme. In Fig. 12 we show an example of a *two schemes* extrapolation procedure, which is performed to gain extra confidence in our results (this refers to computations for $O(80)$ on a 32×32 lattice, which are relevant for [28]).

Appendix C: Auto- and cross-correlations

The matrix $\Sigma_{\Delta\tau}^{-1}(n, m)$ was computed taking into account the auto- and cross-correlations between data evaluated at the same time step. To account for this, the blocking method was used [30]. The different perturbative time series were organized into data blocks, averages were calculated on each block, and then the covariance matrix $\Sigma_{\Delta\tau}(n, m)$ was estimated. This procedure was repeated for increasing block sizes, until variances and covariances of the blocks reached a plateau. Once on the plateau, the block sizes were further increased in fixed steps, up to twice the size at which the plateau was (clearly) reached. The stability of the plateau could thus be verified, and the value of the true covariance $\sigma_{X,Y}^{\text{true}}$ (or the variance $\sigma_{X,X}^{\text{true}}$) was estimated as the average of the points in the plateau region. Estimations of the matrix elements (2, 2), (6, 8), (9, 1) in the $O(15)$ case are displayed in Fig. 11. Additionally, from the value of the variance $\sigma_{X,X}^{\text{true}}$ and the trivial variance σ_X^2 it is possible to derive the value of the integrated autocorrelation time τ_{int} [31]. There are various packages that offer an estimate of τ_{int} through the Gamma Functions method [32, 33] so that some results were double checked, finding full agreement.

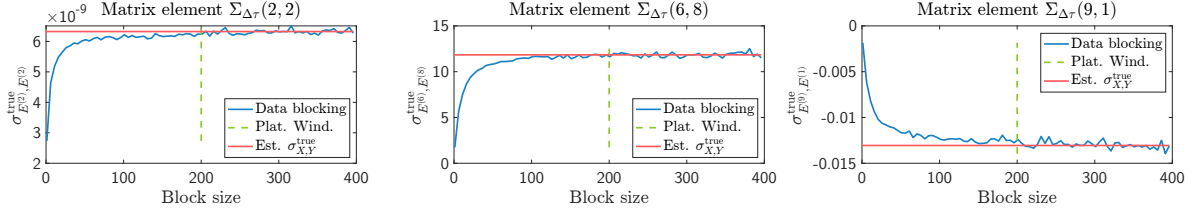


Figure 11: Estimation of the matrix elements $\Sigma_{\Delta\tau}(n, m)$ for the $O(15)$ model at finite time step $\Delta\tau = 0.005$. The plots show the covariance values for each block size in blue. The true covariance was computed in the (plateau) region to the right of the green dashed line. The estimated covariance is the red horizontal line. Each panel displays the loop order pair (n, m) . All block sizes are multiple of 100.

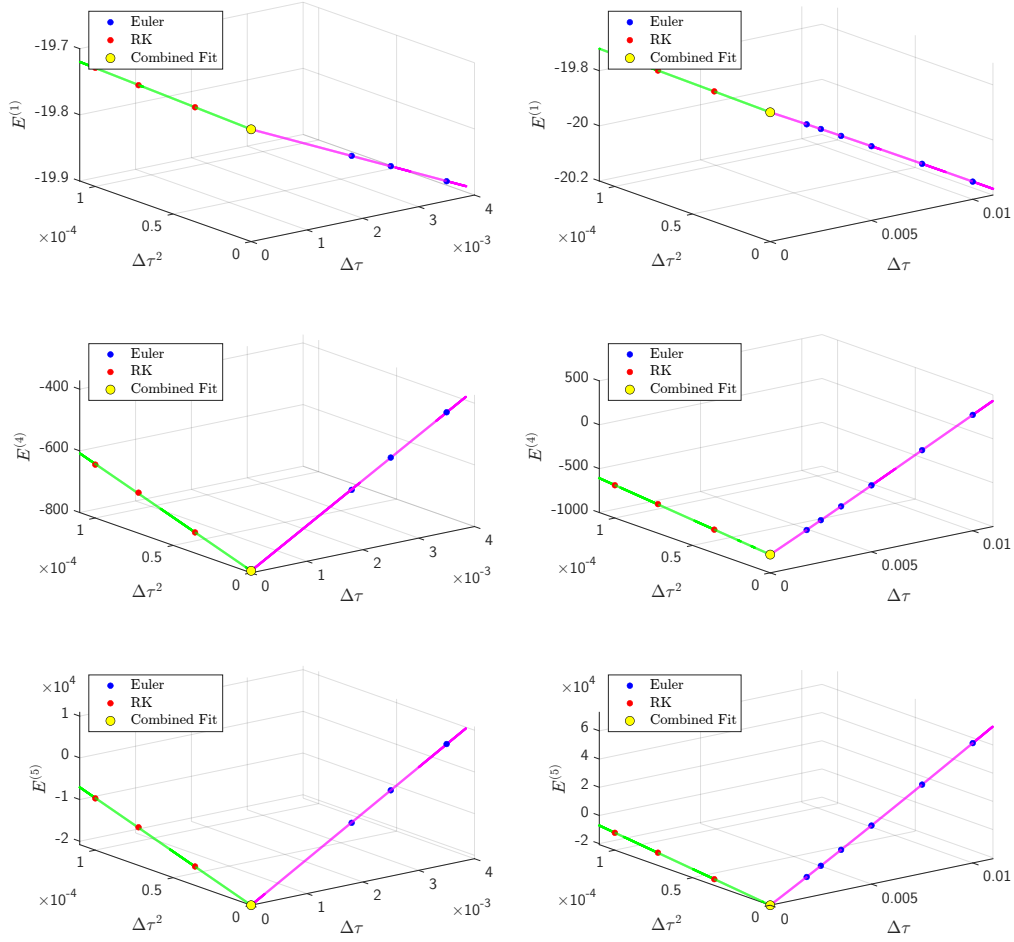


Figure 12: *Two schemes* extrapolation procedure for the $O(80)$ NLSM. Three perturbative orders are displayed on the three rows. Both Euler (blue markers) and Runge Kutta (red markers) integration schemes were used. In the left column, the fitting procedure entails a linear extrapolation in $\Delta\tau$ for Euler (magenta solid line) and a linear extrapolation in $\Delta\tau^2$ for Runge-Kutta (green solid line). In the right column (same color code), a cubic extrapolations in $\Delta\tau$ for the Euler data is performed (taking into account more values of $\Delta\tau$). The values we are interested in are those of the intercepts (yellow markers), resulting from the combined fit.